

DIRECT NUMERICAL SIMULATION OF HYPERSONIC FLOW THROUGH REGULAR AND IRREGULAR POROUS SURFACES

ADRIANO CERMINARA¹, RALF DEITERDING² AND NEIL D. SANDHAM³

Aerodynamics and Flight Mechanics Research Group, University of Southampton,
Southampton, Hampshire, SO17 1 BJ, UK

¹ a.cerminara@soton.ac.uk, ² R.Deiterding@soton.ac.uk, ³ n.sandham@soton.ac.uk

Key words: Fluid Dynamics, Hypersonic Flow, Computational Methods

Abstract. Flow at hypersonic speeds is characterised by severe heat loads at the wall that can lead to the failure of the vehicle structure. Most passive-cooling thermal protection systems (TPS) make use of a low-density porous material to decrease the thermal conductivity and the heat transfer in the inner structure. Porosity plays in turn an important role in active-cooling systems, allowing the coolant gas to be injected into the hot boundary layer, as in the case of transpiration cooling. Thus, the correct design of a TPS requires advanced numerical techniques, for the modeling and meshing of the porous structure as well as for accurate simulation of the flow in the boundary layer and within the pores. In the present work, direct numerical simulations of the Navier-Stokes equations are performed to study a Mach 6 flow over two different surface configurations, namely i) a flat plate with periodic regular pores, and ii) a flat plate with a slot of inner irregular porosity. The simulations are performed through a high-resolution hybrid method, consisting of a 6th order central differencing scheme for the smooth regions of the flow, and a 6th order weighted essentially non-oscillatory (WENO) scheme switched on only in the sharp flow regions. The hybridization minimizes the numerical dissipation while providing numerical stability and computational cost reduction. Moreover, a structured adaptive mesh refinement (SAMR) methodology is used, which dynamically refines the grid by adding consecutive finer grid levels in the local flow regions where sharp gradients are encountered. The SAMR approach, in particular, is crucial for the accurate resolution of the different scales of the flow within the boundary layer and inside the inner porosity layer. A comparison of the main flow features between the case of periodic regular pores and the case of irregular pores is presented, with focus on the radiation of acoustic disturbances in the external field and on the flow characteristics inside and outside the porosity layer. These results demonstrate the code capabilities in performing multiscale DNS simulations of hypersonic flow, resolving both the boundary layer and the flow within the porous layer. As such they provide a basis for future simulations of more complex porous geometries in the context of transpiration-cooling system design for new-generation hypersonic vehicles.

1 INTRODUCTION

Hypersonic flight is characterized by very high values of temperature and heat-flux reached at the wall, which can compromise the structural integrity of the vehicle. In order to reduce the wall heating effects, hypersonic vehicles need an appropriate thermal protection system (TPS) capable of storing, or radiating/dissipating outwards, the high heat load and keeping the surface temperature of the internal structure within tolerable values. For lifting bodies, reusable ceramic-matrix and carbon-carbon composite materials have been shown to be the most suitable materials for the TPS, providing high heat-load storage and thermal resistance capabilities. However, for ballistic reentry bodies, the higher heating loads encountered require the TPS to be formed of non-reusable polymeric-matrix ablative materials. Active cooling, which consists of injecting cold fluid into the boundary layer through localised holes (i.e. ‘film cooling’ [1, 2]) or a porous wall (i.e. ‘transpiration cooling’ [3, 4]) to reduce the wall heat flux, can help meet both the wall-temperature and reusability requirements for hypersonic vehicles in very severe environments, reducing both the thickness and weight of the TPS.

The film cooling technique is commonly used for turbine blades in the form of injection from single holes [5, 6]. However, in this case three-dimensional vorticity structures are generated in the flowfield which can reduce the average cooling effectiveness [7]. In contrast, injection through two-dimensional (2D) slots leads to higher cooling effectiveness by providing a spanwise homogeneous flowfield [8]. This is the form of injection mostly investigated for supersonic flow conditions. Keller and Kloker [8, 9, 10] studied the film cooling properties and main influencing parameters in both laminar and turbulent supersonic boundary layers through direct numerical simulations (DNS). The work of Heufer and Olivier [7] presents a fundamental investigation of film cooling in a laminar supersonic flow over a flat plate with slot injection through both experiments and numerical simulations. From the numerical side, the results for the cooling performance are strongly affected by the way in which blowing is modelled. For example, simulated blowing instead of modelled blowing, as well as the thermal boundary condition at the wall (either isothermal or adiabatic) and the effect of the plenum chamber in the simulation, are all factors that can strongly influence the results [10].

The present work considers the comparison between the case of air injection through regular-shaped equally-spaced holes and the case of injection through an irregular interior porosity layer on the flow features of a three-dimensional (3D) laminar hypersonic boundary layer over a flat plate. Direct numerical simulations are performed through a 6th-order hybrid method [11, 12, 13, 14], combining solution accuracy and numerical stability. The flow features within the pores and in the boundary layer are accurately resolved in a computationally efficient way through the use of an adaptive mesh refinement (AMR) methodology, which locally adds consecutive refinement levels in the regions of high gradients. This study supports current experimental investigations of film cooling over a flat plate in hypersonic flow, and serves as a basis for future calibrated studies aimed at analyzing the effectiveness of transpiration cooling systems.

2 NUMERICAL METHOD

2.1 Governing equations

We consider numerical solutions of the three-dimensional Navier-Stokes equations for compressible flows, written in conservation form, under the assumption of a perfect gas. The set of non-dimensional conservation equations in Cartesian coordinates can be written as

$$\frac{\partial \mathbf{Q}}{\partial t} + \frac{\partial(\mathbf{F}_j)}{\partial x_j} = 0 .$$

In the equation above, \mathbf{Q} is the vector of the conservative variables, while \mathbf{F}_j is the vector of the fluxes in Cartesian coordinates. The components of the vectors of the system in conservative form are

$$\mathbf{Q} = \begin{bmatrix} \rho \\ \rho u \\ \rho v \\ \rho w \\ \rho E \end{bmatrix}$$

and

$$\mathbf{F}_j = \begin{bmatrix} \rho u_j \\ \rho u u_j + \delta_{1j} p - \frac{1}{Re} \tau_{1j} \\ \rho v u_j + \delta_{2j} p - \frac{1}{Re} \tau_{2j} \\ \rho w u_j + \delta_{3j} p - \frac{1}{Re} \tau_{3j} \\ \rho \left(E + \frac{p}{\rho} \right) u_j - \frac{1}{Re} \left(u \tau_{1j} + v \tau_{2j} + w \tau_{3j} + \frac{\mu}{(\gamma - 1) Pr M^2} \frac{\partial T}{\partial x_j} \right) \end{bmatrix} .$$

The terms ρ , ρu , ρv , ρw and ρE are the conservative variables of the system of equations, where ρ is the density, u , v and w are the velocity components respectively in the x , y and z directions, and E is the total energy per unit mass. In the flux vectors, the terms p , T , τ_{ij} , and μ are respectively the pressure, the temperature, the components of the viscous stress tensor, and the dynamic viscosity of the flow. The non-dimensional quantities are obtained through normalisation of the dimensional variables with their freestream reference values: the velocity components are normalised with the freestream main velocity (U_∞^*), the density is normalised with the freestream density (ρ_∞^*), the viscosity is normalised with the freestream dynamic viscosity (μ_∞^*), the temperature is normalised

with the freestream temperature (T_∞^*), the total energy is normalised with the square of the freestream mean velocity (U_∞^{*2}), while the pressure and viscous stresses are normalised with the term $\rho_\infty^* U_\infty^{*2}$, related to the freestream dynamic pressure. Note that the superscript (*) is used to denote dimensional values. The characteristic length chosen to normalise the length scales is the boundary-layer displacement thickness (δ^*). The time scales are normalised with respect to the fluid dynamic characteristic time (δ^*/U_∞^*), based on the velocity of the undisturbed flow and on the characteristic length. The terms Re , Pr , M , and γ are respectively the Reynolds, Prandtl and Mach numbers, and the ratio of specific heats ($\gamma = c_p^*/c_v^*$), i.e. the dimensionless parameters of the flow. The Reynolds number is defined with respect to the boundary-layer displacement thickness of the similarity solution, as $Re = (\rho_\infty^* U_\infty^* \delta^*)/\mu_\infty^*$; the Prandtl number is set to 0.72 for air, and γ is equal to 1.4, as we are considering a perfect gas model. The dynamic viscosity is, in turn, expressed in terms of temperature by Sutherland's law

$$\mu = T^{3/2} \frac{1 + C}{T + C} ,$$

where the constant C represents the ratio between the Sutherland's constant (set to 110.4 K) and the reference temperature in the freestream T_∞^* . The viscous stresses are defined in terms of the velocity derivatives, under the assumption of a Newtonian fluid, as

$$\tau_{ij} = \mu \left[\frac{\partial u_i}{\partial x_j} + \frac{\partial u_j}{\partial x_i} - \frac{2}{3} \delta_{ij} \frac{\partial u_k}{\partial x_k} \right] .$$

We also need a relation linking the total energy to the temperature, which in non-dimensional form can be expressed as

$$E = \frac{T}{\gamma(\gamma - 1)M^2} + \frac{1}{2} (u^2 + v^2 + w^2) .$$

Finally, the system of equations is closed by the equation of state for a perfect gas

$$p = \frac{1}{\gamma M^2} \rho T .$$

2.2 Code features

The numerical simulations have been carried out using the code AMROC [12, 13] (Adaptive Mesh Refinement in Object-oriented C++), which uses a hybrid WENO-centred-difference (WENO-CD) scheme in conjunction with a structured adaptive mesh refinement (SAMR) approach. The implementation relative to the base central scheme is equipped with the option to be tuned (or optimised) for spectral resolution improvement, which denotes the scheme as WENO-tuned-centred-difference (WENO-TCD), as described by Hill and Pullin [11]. The shock-capturing filter, namely the WENO scheme, corresponds to the type of WENO-symmetric-order-optimised (WENO-SYMOO) scheme as shown by Martin *et al.* [15]. The schemes are integrated with a switching function that turns on/off the WENO method at discontinuities/smooth regions.

The base scheme (central scheme) has been proven to have a maximum formal order of accuracy of 6, corresponding to a 7-point stencil, with relative stencil coefficients as in Ziegler *et al.* [14]. The order of accuracy can be properly specified, which changes the stencil, and can be also reduced (keeping constant the stencil) for optimisation of the bandwidth resolution capabilities. For example, considering the 7-point stencil, if the optimisation option is specified, the corresponding scheme will be a 4-th order accurate scheme with optimised bandwidth properties [11], thus a minimum dispersion error of the modified wavenumber, suitable for LES (Large-Eddy-Simulation) simulations. Details of the WENO-CD scheme can be found in Cerminara *et al.* [16].

3 RESULTS

3.1 Flat plate with periodic regular pores

Preliminary two-dimensional (2D) simulations for the present case, aimed at validating the code, performing a grid resolution study and testing the computational performance, were shown in the work of Cerminara *et al.* [16]. The Mach number is 6, the Reynolds number based on the initial boundary layer displacement thickness is 6000, the freestream temperature is $T_\infty = 216.65$ K, and the wall temperature is fixed to the adiabatic wall temperature, i.e. $T_w^* = T_{ad}^* = 7.027T_\infty^* = 1522.4$ K. The reference length is the displacement thickness of the initial laminar boundary layer of the similarity solutions, through which the flowfield is initialised in our numerical simulations.

Simulations were performed for a 3D case with 16 square-shaped holes, whose domain shown in figure 1 with a mesh size of $128 \times 660 \times 128$. The 6th-order WENO-CD method was used. Injection boundary conditions were used to the bottom of each pore, with a fixed parabolic profile of the vertical velocity and maximum injection velocity of $v_{max} = 0.3$, to simulate air-into-air injection with a temperature of $0.8T_w$.

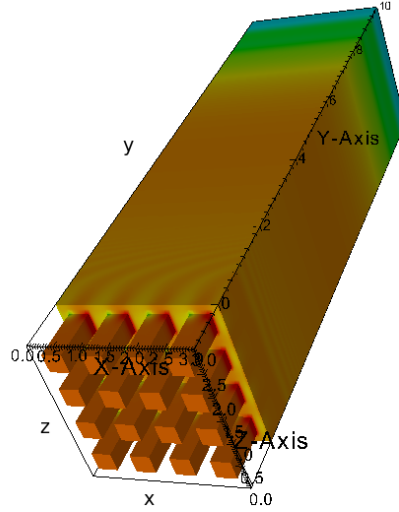


Figure 1: 3D view of the domain for the flat plate with periodic holes. Plotted variable: pressure - no injection

Figure 2 shows results for the temperature field and the vertical velocity field on the xy plane at the spanwise position $z = 1.5$. As can be seen, the maximum vertical velocity is reached at the pore edges, due to the further expansion taking place into the pores as the fluid moves outwards. The fluid released inside the boundary layer then decelerates and is deflected towards the mean stream direction. The temperature plot shows that the minimum temperature is reached at the pore edges, consistent with the maximum velocity related to the expansion. The boundary layer near the wall is affected by the cooling effect of the colder injection flow, whereas a high temperature peak is located in a narrow layer at the boundary layer edge. This is associated with the compression of the fluid towards the boundary layer edge due to the vertical flow with high injection speed.

Figures 3 and 4 show the density and pressure fields respectively, on a xy plane (at $z = 1.5$) and on a zy plane (at $x = 1.5$). It is evident that the flow within the pores is characterised by high density and high pressure values, and that the jets provide a considerable boundary-layer distortion in the spanwise direction. An oscillatory behaviour of the pressure is observed along the axis of each pore near the pore edges, and outside the boundary layer weaker pressure waves are formed, which represent acoustic waves radiated into the freestream and travelling downstream with an inclination equal to the Mach angle.

As can be seen, the details of the flow features for fluid injection into a hypersonic boundary layer are well resolved by the high-resolution WENO-CD method, which demonstrates the capabilities of the considered method in the context of DNS of hypersonic flow over porous surfaces.

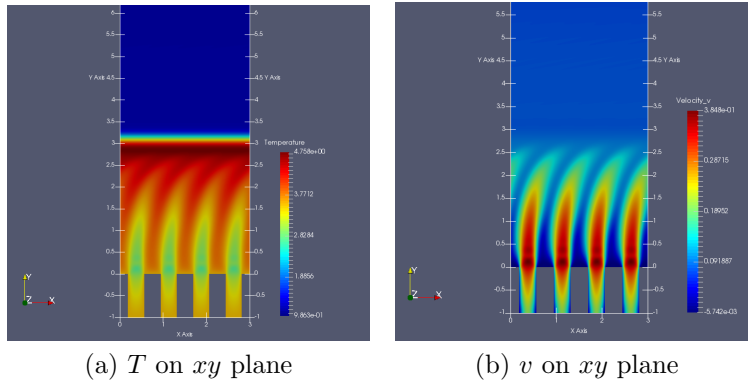


Figure 2: Temperature (a) and vertical velocity (b) fields on the xy plane at $z = 1.5$

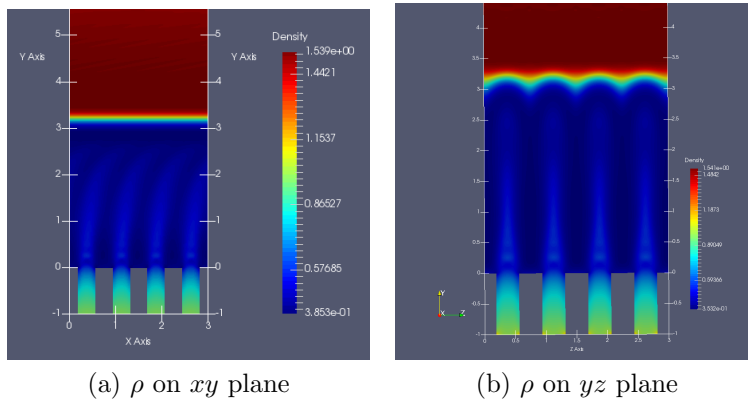


Figure 3: Density field on the xy plane at $z = 1.5$ (a) and on the yz plane at $x = 1.5$ (b)

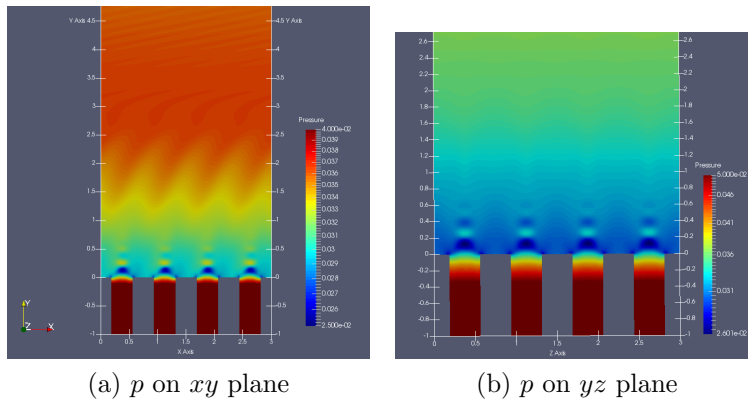


Figure 4: Pressure field on the xy plane at $z = 1.5$ (a) and on the yz plane at $x = 1.5$ (b)

3.2 Flat plate with irregular porosity slot

The considered configuration in this section is a 3D flat plate with a layer of irregular porosity. The freestream conditions are the same of Section 3.1 except for the Reynolds number, which is imposed as $Re = 20000$ for this case. Periodic boundary conditions are used only at the side boundaries, whereas an extrapolation condition is applied the inlet (located at $x = -3$), and a standard outflow condition is applied at the outlet (located at $x = 4$). The irregular porosity consists of a prescribed number of spherical solid elements inserted into the slot through an immersed boundary method, on which no-slip wall boundary conditions are applied. A total of 400 elements are used, each one with a radius of 0.07, and with a prescribed position in space. This arrangement of spherical particles is used as an initial attempt to reproduce more realistic porous surfaces.

Figure 5 shows the pressure field for a case without injection. Here, the thickness of the slot is 1, and the red spherical particles represent the solid particles inserted into the slot. As can be seen, strong acoustic waves are formed at the slot corners and transmitted in the freestream, where they propagate downstream at the Mach angle. This feature was observed also for the case of regular pores. The pressure field within the pores appears approximately uniform. The mesh size for the present simulation is $140 \times 120 \times 20$, and 3 overall grid levels were used for the adaptive mesh refinement. Figure 6 shows details of the local temperature variation through the porous layer, as well as the mesh refinement levels. As it is evident, the temperature peaks are located in the regions of higher density of the solid particles. The finer grid levels are added inside the porous layer to accurately resolve the flow features within the porosity length scales.

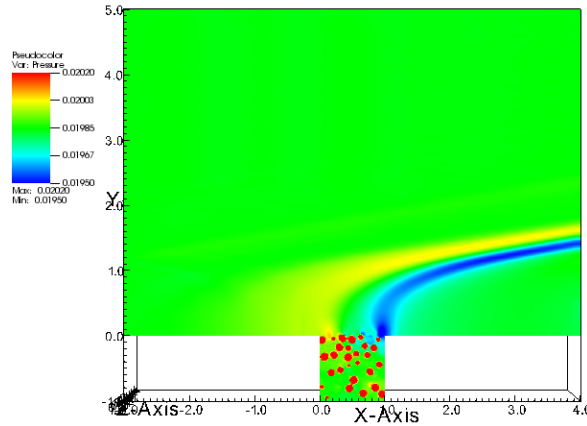


Figure 5: Pressure field for configuration with irregular porosity layer - no injection

Figure 7a shows the pressure field in the case of injection. In this configuration, the boundary conditions prescribed on the bottom boundary simulate the conditions in the plenum chamber. In particular, at this boundary the velocity is set to zero and pressure and temperature are fixed to the values of $p_0 = 1.5p_\infty$ and $T_0 = 300$ K. The thickness of the slot is now 1.5, allowing some gap between the plenum chamber boundary and the beginning of the porosity layer. A strong pressure gradient is generated across the porous

layer, with maximum located at the bottom boundary, which forces vertical flow from the plenum chamber towards the boundary layer.

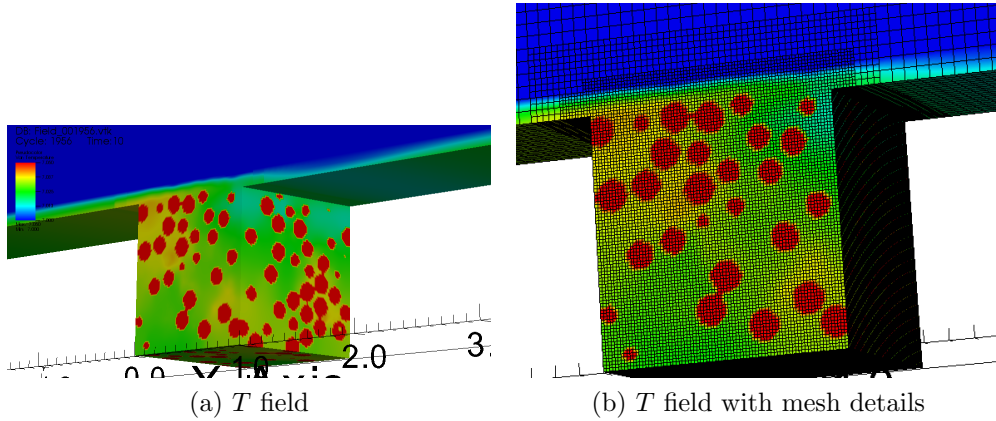


Figure 6: View of the temperature field in the inner porosity layer without (a) and with (b) mesh details

Figure 7b shows a 3D view of the pressure field, which highlights the 3D non-uniformity of the pressure within the pores.

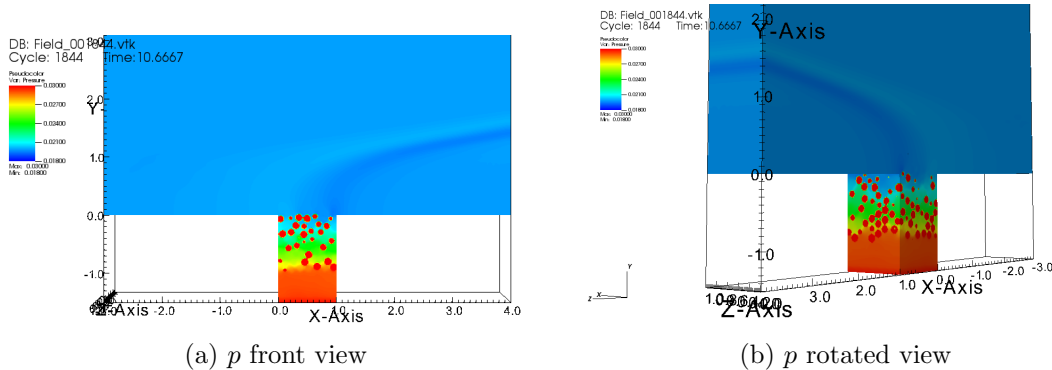


Figure 7: Pressure field for configuration with irregular porosity layer and injection

Figures 8a shows the vertical velocity field. It is possible to notice the details of the vertical flow through the pores. The maximum of the velocity appears to be located between the porous layer and the bottom boundary. Figure 8b shows the streamwise velocity field, which indicates that no evident distortion of the boundary layer is produced, due to the low injection rates imposed by the relatively low pressure value inside the plenum chamber, as well as to the resistance to the vertical flow impressed by the porosity layer. Finally, figures 9a and 9b show results for the pressure and vertical velocity fields at the same injection conditions, but for a different geometrical configuration. In this case, the thickness of the slot is 2, and the density of the solid particles within the slot was

reduced by enlarging the maximum volume containing the particles (in all the directions) by a scaling factor equal to 1.5. Figure 9a shows that a lower pressure gradient is formed across the porous layer, compared to the previous higher-particle-density case, which is a result of a higher penetration capability of the injected flow into the boundary layer. This is also observed in the vertical velocity field (9b), where the maximum velocity is reached near the upper surface of the porous layer. Moreover, it is evident that the vertical flow coming out from the porous layer produces a high pressure region inside the boundary layer just upstream of the porous slot, and the formation of a stronger and thicker compression wave transmitted in the freestream.

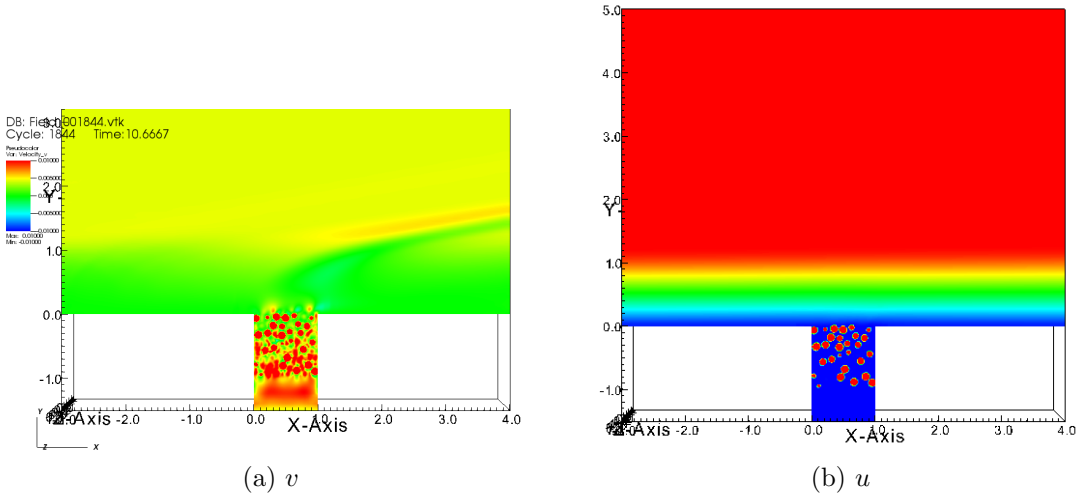


Figure 8: Vertical (a) and streamwise (b) velocity fields for configuration with irregular porosity layer and injection

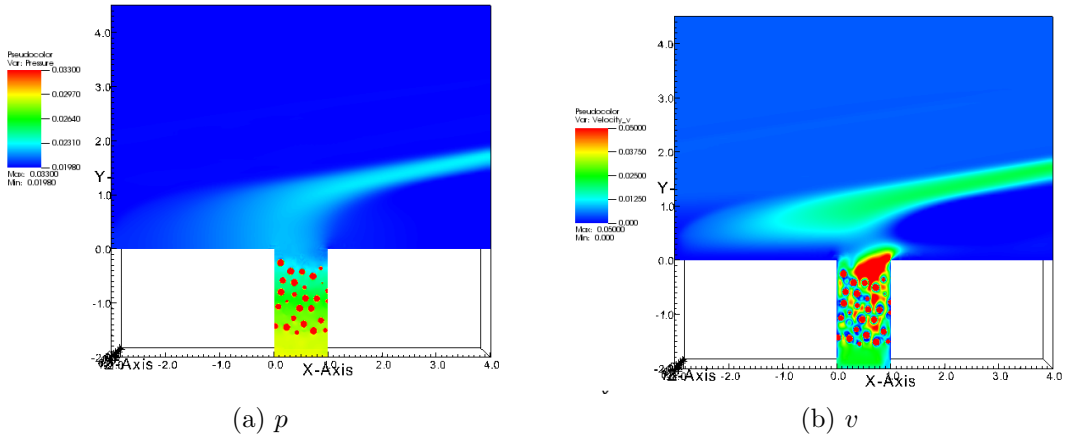


Figure 9: Pressure (a) and vertical velocity (b) fields for configuration with lower particle-density irregular porosity layer and injection

4 CONCLUSION

DNS simulations were carried out to study the flow features of a Mach 6 hypersonic flow over a flat plate with regular periodic pores and an irregular porosity layer, with and without injection. In the case of an irregular porosity layer with injection, the presence of the plenum chamber is simulated at the bottom boundary through prescribed plenum boundary conditions.

Results for both the cases of regular holes and irregular porosity, obtained through a high-resolution WENO-CD method, showed well resolved flow features of the fluid injection into a hypersonic boundary layer. The flow features within the porous layer were accurately captured in a computationally efficient way through the adaptive mesh refinement approach, by adding consecutive refinement levels within the pores. These results demonstrate the capabilities of the considered method to efficiently execute DNS simulations in hypersonic flow for complex porous surfaces, and represent a first approach to the simulation of more realistic porous media for transpiration cooling applications.

ACKNOWLEDGMENTS

The authors would like to acknowledge support from EPSRC (Engineering and Physical Sciences Research Council) under the Grant No. EP/P000878/1.

REFERENCES

- [1] Fitt, A. D., Ockendon, J. R., and Jones, T. V., *Aerodynamics of slot-film cooling: theory and experiment*, Journal of Fluid Mechanics, 160, November 1985, pp. 15-27.
- [2] Fitt, A. D., and Wilmott, P., *Slot film cooling - the effect of separation angle*, Acta Mechanica, 103.1-4, 1994, pp. 79-88.
- [3] Meinert, J., Huhn, J., Serbest, E., and Haidn, O. J., *Turbulent boundary layers with foreign gas transpiration*, Journal of Spacecraft and Rockets, 38.2, 2001, pp. 191-198.
- [4] Gülhan, A., and Braun, S., *An experimental study on the efficiency of transpiration cooling in laminar and turbulent hypersonic flows*, Experiments in fluids, 50.3, 2011, pp. 509-525.
- [5] Wittig, S., Schulz, A., Gritsch, M., and Thole, K. A., *Transonic film-cooling investigations: effects of hole shapes and orientations*, American Society of Mechanical Engineers, International Gas Turbine and Aeroengine Congress and Exhibition, 96-GT-222, June 1996.
- [6] Baldauf, S., Schulz, A., and Wittig, S., *High-resolution measurements of local heat transfer coefficients from discrete hole film cooling*, Transactions of the ASME-T-Journal of Turbomachinery, 123.4, 2001, pp. 749-757.

- [7] Heufer, K. A., and Olivier, H., *Experimental and numerical study of cooling gas injection in laminar supersonic flow*, AIAA Journal, 46.11, 2008, pp. 2741-2751.
- [8] Keller, M. A., and Kloker, M. J. *Direct Numerical Simulation of Foreign-Gas Film Cooling in Supersonic Boundary-Layer Flow*, AIAA Journal, 55.1, 2017, pp. 99-111.
- [9] Keller, M. A., Kloker, M. J., and Olivier, H., *Influence of cooling-gas properties on film-cooling effectiveness in supersonic flow*, Journal of Spacecraft and Rockets, 52.5, 2015, pp. 1443-1455.
- [10] Keller, M. A., and Kloker, M. J., *Effusion cooling and flow tripping in laminar supersonic boundary-layer flow*, AIAA Journal, 53.4, 2015, pp. 902-919.
- [11] Hill, D.J., and Pullin, D.I., *Hybrid tuned center-difference-WENO method for large eddy simulations in the presence of strong shocks*, Journal of Computational Physics, 194.2, 2004, pp. 435-450.
- [12] Deiterding, R., *Construction and application of an AMR algorithm for distributed memory computers*, Adaptive Mesh Refinement - Theory and Applications, Lecture Notes in Computational Science and Engineering, 41, 2005, Springer, pp. 361-372.
- [13] Deiterding, R., *Detonation structure simulation with AMROC*, High Performance Computing and Communications, Lecture Notes in Computer Science, 3726, 2005, Springer, pp. 916-927.
- [14] Ziegler, J. L., Deiterding, R., Shepherd, J. E., and Pullin, D. I., *An adaptive high-order hybrid scheme for compressive, viscous flows with detailed chemistry*, Journal of Computational Physics, 230.20, 2011, pp. 7598-7630.
- [15] Martn, M. P., Taylor, E. M., Wu, M., and Weirs, V. G., *A bandwidth-optimized WENO scheme for the effective direct numerical simulation of compressible turbulence*, Journal of Computational Physics, 220.1, 2006, pp. 270-289.
- [16] Cerminara, A., Deiterding, R., and Sandham, N. D., *DNS of Hypersonic Flow over Porous Surfaces with a Hybrid Method*, AIAA 2018-0600 Pap., AIAA Aerospace Sciences Meeting, SciTech Forum, Kissimmee (FL), 2018